METALS AND MATERIALS International, Vol. 11, No. 1 (2005), pp. 19~27

Design of Bulk Metallic Glasses with High Glass Forming Ability and Enhancement of Plasticity in Metallic Glass Matrix Composites: A Review

E. S. Park and D. H. Kim*

Center for Non-crystalline Materials, Department of Metallurgical Engineering, Yonsei University
134 Shinchon-dong, Seodaemoon-gu, Seoul 120-749 Korea

To overcome some of the limits of existing metallic alloys, a new alloy design concept has been introduced recently in order to control the crystallinity, i.e. to utilize crystalline, quasicrystalline, and amorphous structures. In particular, bulk metallic glasses (BMGs) receive great attention because of their unique properties due to their different atomic configuration. Recently, significant progress in enhancing glass forming ability (GFA) has led to the fabrication of BMGs having potential for application as structural and functional materials. Moreover, successful design of BMG matrix composite microstructure suggests that the plasticity of BMGs can be controlled properly. In this review article, we introduce recent research results on the design of BMGs with high GFA and on the enhancement of plasticity in metallic glass matrix composites.

Keywords: bulk metallic glasses (BMGs), glass forming ability (GFA), critical cooling rate (CCR), plasticity, metallic glass matrix composites (MGMCs)

1. INTRODUCTION

Following Duwez and co-workers report in the early 1960s on the formation of metallic glass (MG) in the Au-Si system by the rapid quenching technique (RQT) [1], there has been considerable progress in understanding of RQT and alloy development for MG. MG alloy shows characteristic physical properties such as high strength, corrosion resistance, and electromagnetic properties, which are significantly different from the corresponding crystalline alloys due to the different atomic configuration [2]. Owing to the requirement of rapid solidification, however, MGs can be produced in the form of either a thin ribbon or fine powders. This limits wide application of MGs except for special purposes such as magnetic materials and brazing.

Recently, several multi-component alloys (MCAs) capable of solidifying into glass at a relatively low cooling rate have been developed. The development of MCAs requiring very low cooling rates of only about $1\sim10^2$ K/s to vitrify without crystallization permits the production of large-scale bulk metallic glass (BMG) samples with diameters as large as 30 mm [3]. Several BMGs have been developed in Ni-based [4], Pd-based [5], Fe-based [6,7], Cu-based [8], Ti-based [9], Ca-based [10], and Mg-based alloy systems [11].

BMGs are known to have unique mechanical properties, including high strength, relatively low Youngs modulus, and excellent elastic behavior [12]. However, they show little overall room temperature plasticity, but rather deform by highly localized shear banding, resulting in catastrophic failure [13]. Recent attempts to improve the ductility of BMGs have focused on the preparation of composite materials exhibiting a microstructure consisting of crystalline phases such as particles [14], fibers [15] or *in-situ* formed precipitates [16] dispersed in the metallic glass matrix (MGM). The metallic glass matrix composites (MGMCs) have been found to exhibit enhanced plasticity, not generally observed in monolithic BMGs [17]. This deformation behavior possibly stems from the formation of multiple shear bands initiated at the interface between the reinforcing agent and the MGM, and their confinement in MGMCs [18]. The improved ductility may open the possibility to overcome the limited applications of monolithic BMGs, which fail catastrophically with little plastic elongation in an apparently brittle manner. However, only a few alloy systems with high glass forming ability (GFA), such as, Zr- [19,20] and Ti- [21] based BMGs, have been obtained as MGMCs.

Recently, it has been shown that the production of BMGs by consolidation of amorphous powders has promising and important practical applications in the near-net-shape fabrication of components with novel properties [22]. Several alloy systems based on Ti [9,23], Cu [8], and Ni [4,24] have a high GFA, thus enabling the fabrication of ingots based on a Cu-mold casting method. This flexible processing method can substantially ease the limitations in sample shape and

*Corresponding author: dohkim@yonsei.ac.kr

size. The successful consolidation of amorphous powders has been reported in several alloy systems such as Zr-, Cu- and Ni- based systems [22,25,26].

The main aim of this review article is to introduce recent research results on the design of bulk metallic glasses with high glass forming ability in Ca-, Mg-, Ni-, Cu-, and Ti-based alloys and on the enhancement of plasticity in metallic glass matrix composites.

2. Ca-BASED BMGS

The glass forming ability (GFA) of an alloy system mainly depends on the stability of the under-cooled liquid or the difficulty in forming competing phases during solidification. In general, higher degrees of chemical complexity are required for metallic alloys to exhibit good GFA. However, recently, ternary alloys such as Cu-(Zr, Hf)-Ti [27], Cu-Zr-Al [28], Ni-Nb-(Sn [29], Ti [30], Ta [31]), and Mg-Cu-(Y [32], Gd [33]) have been reported to have GFA high enough to form BMGs. These simple ternary alloys are more suitable for commercial use, and provide a good opportunity for the study of glass-forming mechanisms. Although most BMGs must be fabricated under a controlled inert atmosphere in an evacuated closed chamber, some ternary BMGs such as in the Mg-Cu-Gd system can be fabricated by a conventional Cu-mold casting method in air atmosphere. Such a rapid and simple production technique will facilitate the widespread use of BMGs in industrial products.

Ca-based binary alloys such as Ca-Al, Ca-Mg, Ca-Zn, and Ca-Cu alloys have been reported to form amorphous phase by rapid solidification method. Recently, Ca-Mg-M (M: Cu, Ni, Ag, Zn) ternary alloys were reported to show a large supercooled liquid region (SLR) and a high GFA [34,35,10]. The maximum rod diameters for the formation of a glassy phase were 4 mm for $Ca_{60}Mg_{20}Ag_{20}$ and 7 mm for $Ca_{57}Mg_{19}Cu_{24}$. In particular, the Ca-Mg-Zn alloy system has received attention because it can be fabricated into BMG samples under air atmosphere, exhibiting high GFA. Recently, it was reported that a $Ca_{65}Mg_{15}Zn_{20}$ alloy was utilized to form a BMG sample with a diameter of 15 mm by a conventional Cu-mold casting method in air atmosphere [10]. Fig. 1 shows the cooling curves measured at the center of three transverse cross-sections. No evidence of heat release due to recalescence was observed, again confirming the formation of a single amorphous phase. The cooling rates measured at the center of the bottom, middle, and top positions were ~149 K/s, ~93 K/s, and ~20 K/s, respectively. The cooling rate for glass formation was obtained from $(T_l-T_g)/\Delta t$, where Δt is the range of time from T_l to T_g. Since the whole as-cast ingot has an amorphous structure, the CCR for glass formation in the $Ca_{65}Mg_{15}Zn_{20}$ alloy is less than ~20 K/s. The critical cooling rate for glass transition can be calculated by building an integrated transformation curve, which is constructed by combining the continuous cooling transformation (CCT) and continuous heating transformation (CHT) curves [36]. The CCT and CHT curves can be calculated from experimental measurements of cooling rate dependence of solidification onset temperature using classical nucleation kinetics and heating rate dependence of crystallization onset temperature by extension of the Kissinger method, respectively. The critical cooling rate estimated from the intersection point of the CCT and CHT curves is 28 K/s. This calculated critical cooling rate is in good agreement with the measured value of about 20 K/s.

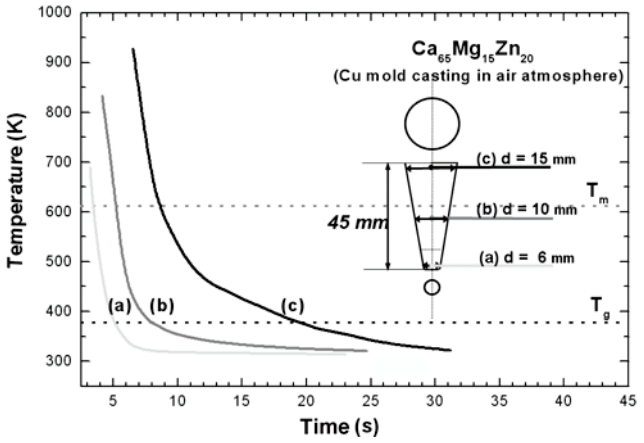

Fig. 1. Cooling curves obtained from different positions: top, middle, and bottom positions of the cone-shaped mold.

The high GFA in the Ca-Mg-Zn alloy system can be explained by the empirical rules: (1) large atomic size difference between the alloy elements (Ca: 1.97 Å; Mg: 1.60 Å; Zn: 1.38 Å), (2) large negative mixing enthalpy between the alloy elements (Ca-Mg: −20 J/mol; Ca-Zn: −72 J/mol; Mg-Zn: −13 J/mol), and (3) existence of a deep ternary eutectic reaction in the Ca-rich composition range [37]. The decrease in melting point indicates that the liquid phase is stabilized with respect to competing crystalline phases. A large atomic size difference between constituent elements is favorable to increase the atomic packing density of the liquid structure, destabilizing the competing crystalline phase against glass formation. The increase in the packing density of atomic configurations is supported by the very small change in density of the multicomponent amorphous alloys upon crystallization. The density of the $Ca_{65}Mg_{15}Zn_{20}$ alloy was 2.140 g/cm^3 in the amorphous state, and 2.147 g/cm^3 in the crystallized state. The change of density upon full crystallization was 0.3 %, which is much smaller than that for an amorphous alloy requiring high cooling rate for the formation of the amorphous phase, i.e., 2~3 % [38]. This observation suggests that the atomic configuration in the $Ca_{65}Mg_{15}Zn_{20}$ amorphous alloy has a high packing density, which partly contributes to the improved glass forming ability.

The compressive strength and density of the amorphous $Ca_{65}Mg_{15}Zn_{20}$ alloy are 608 MPa and 2.140 g/cm^3, respec-

tively. Therefore, the specific strength of the amorphous $Ca_{65}Mg_{15}Zn_{20}$ alloy is 2.81×10^5 N·m/kg [39]. Although Ca-based BMG does not exhibit significantly higher absolute strength than other bulk metallic glasses, the high specific strength value implies that Ca-based BMG can provide adequate strength in a low-density configuration.

3. Mg-BASED BMGS

Mg-TM-RE (TM: transition metal such as Ni, Cu, Zn; RE: rare-earth metal such as Y) alloy systems exhibit a large SLR and high GFA [40,41]. Since Inoue and Masumoto [42] first reported the formation of BMG in $Mg_{65}Cu_{25}Y_{10}$, enhancement of GFA has been reported in various Mg-Cu-Y-X (X=Ag, Pd, Zn) alloy systems [43-46]. The maximum diameter among BMG samples fabricated by injection casting is 6 mm for $Mg_{65}Cu_{15}Ag_{10}Y_{10}$ alloy [43]. Recently, it has also been reported that $Mg_{65}Cu_{25}Gd_{10}$ ternary alloy has a significantly improved GFA, enabling the fabrication of a BMG sample with a maximum diameter of 8 mm by conventional Cu-mold casting method in air atmosphere [33]. The electronic band structure of MGs is known to be dependent on the type of short-range order [47]. For Ni-Fe-B MGs, it has been shown theoretically [48] and experimentally [49-52] that chemical ordering occurs by the preferential bonding interaction between B and Ni due to the difference in the electronic structure of Ni($3d^8 4s^2$) and Fe($3d^6 4s^2$), although Ni and Fe have similar Goldschmidt atomic radius (Ni: 0.125 nm, Fe: 0.128 nm) and heat of mixing with B (Ni-B: -9 kJ/mol, Fe-B: -11 kJ/mol). Thus, the difference in electronic configuration between Y ($4d^1 5s^2$) and Gd ($4f^7 5d^1 6s^2$) may result in a certain change of the short-range order in a super-cooled liquid with substitution of Y by Gd in $Mg_{65}Cu_{25}Y_{10}$ alloy, which results in a different crystallization route and favors glass formation.

The partial substitution of Cu by Ag and Pd improves the GFA of the $Mg_{65}Cu_{25}Gd_{10}$ ternary alloy. The $Mg_{65}Cu_{15}Ag_5Pd_5Gd_{10}$ BMG sample 10 mm in diameter is fabricated by a conventional Cu-mold casting method in air atmosphere [53]. Fig. 2 shows the XRD patterns of transverse cross-sections with diameters of 10, 10.5, and 11 mm of an as-cast cone-shaped $Mg_{65}Cu_{15}Ag_5Pd_5Gd_{10}$ ingot. The XRD pattern of the cross-section with 10 mm in diameter exhibits a broad diffraction peak characteristic of MGs, with no evidence of any crystalline peaks. For the cross-sections with 10.5 and 11 mm in diameter, the XRD patterns show sharp peaks from the crystalline phase superimposed on a broad halo peak, indicating the coexistence of crystalline and amorphous phases. The crystalline phases were identified as MgGd, CuGd, Cu_3Pd, and Mg_2Cu phases, as marked in the XRD trace. The DSC analysis from the center to the edge of a thin slice a 10 mm in diameter and 2.5 mm in thickness showed the same results as the as-melt spun ribbon (not shown), confirming a fully amorphous structure.

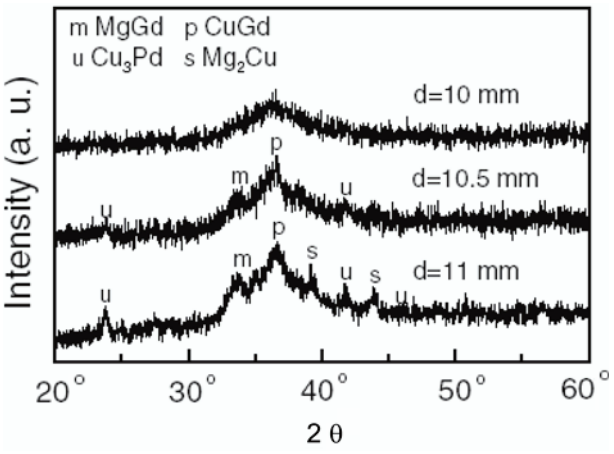

Fig. 2. XRD patterns obtained from the transverse cross-sections of as-cast $Mg_{65}Cu_{15}Ag_5Pd_5Gd_{10}$ ingot with diameters of 10, 10.5, and 11 mm.

Partial substitution of Y by Gd in $Mg_{65}Cu_{15}Ag_{10}Y_{10}$ alloy improves the GFA and mechanical properties [54]. The $Mg_{65}Cu_{15}Ag_{10}Y_2Gd_8$ alloy enables the fabrication of BMG with a diameter of 9 mm by the conventional Cu-mold casting method in air atmosphere. The increase in GFA by the partial substitution of Y by Gd appears to be related with the reduced melting temperature. The compressive fracture strength (σ_f) and fracture elongation (ε_f) for the $Mg_{65}Cu_{15}Ag_{10}Y_2Gd_8$ BMG sample were 956 MPa and 1.6 %, respectively. Young's modulus calculated from the stress-strain curve was 72 GPa.

4. Ni-BASED BMGS

Although many Ni-based amorphous alloys have been produced by RQTs [55,56], Ni-based BMG alloys have only recently been reported, by Inoue *et. al.* Fully amorphous rods with a maximum diameter of 1mm have been prepared in a Ni-Nb-Cr-Mo-P-B system [4], containing large additions of P and B (~20 at.% in total). However, the addition of a large amount of P and B has economical and technological drawbacks. For example, due to the high vapor pressure of P, specific facilities are required during the P addition into melts. Based on the three empirical rules for having large GFA, the ternary Ni-Ti-Zr alloy system was selected as a candidate to exhibit high GFA as a result of the large atomic size difference and strong negative interaction between constituting elements [57]. The ternary MG specimen shows clear glass transition behavior during continuous heating, indicating higher GFA than binary alloys. Further GFA was achieved by addition of Si and Sn. The temperature range for SLR, which is often quoted as the parameter representing GFA, increased from 14 K for $Ni_{59}Zr_{20}Ti_{21}$ to 46 K for $Ni_{59}Zr_{20}Ti_{16}Si_5$ and 58 K for $Ni_{59}Zr_{20}Ti_{16}Si_2Sn_3$ alloy. Fully amorphous rods with a diameter of 2 and 3 mm were obtained, respectively, by injection casting of $Ni_{59}Zr_{20}Ti_{16}Si_5$ and $Ni_{59}Zr_{20}Ti_{16}Si_2Sn_3$

alloys [58]. The addition of Nb in Ni-Zr-Ti-Si-Sn alloy improves the GFA (D_{max}=5 mm, D_{max}: maximum diameter for glass formation by injection casting), and widens the composition range for bulk glass formation with D_{max}>2 mm [59]. Glassy rods with diameter of 5 mm, the largest size reported for Ni-based BMG to date, are fabricated at a composition of $Ni_{59}Zr_{16}Ti_{13}Si_3Sn_2Nb_7$ and $Ni_{59}Zr_{19}Ti_{11}Si_3Sn_2Nb_6$. The compositions of the alloys (D_{max}>2 mm) are closer to the pseudo-eutectic composition than that of the alloy without Nb, thus improving the GFA. The CCR for glass formation (D_{max}=5 mm) is estimated to be on the order of ~ 40 K/s.

In order to overcome the limitation of Ni-based section size of bulk amorphous alloy, warm consolidation has been performed for gas atomized amorphous $Ni_{59}Zr_{20}Ti_{16}Si_2Sn_3$ powder [26]. Amorphous rod specimens with diameter 10 mm have been successfully fabricated by warm extrusion with an extrusion ratio of 5. The extruded amorphous alloy showed compressive fracture strength of about 2 GPa, which is slightly smaller than that for an injection-cast rod specimen, i.e., 2.2 GPa. No fracture occurs along the boundaries between prior particle boundaries. This is attributed to good bonding between the particles. The high strength appears to originate from the good particle bonding. Vein patterns, a typical fracture mode characteristic of amorphous alloys, are clearly observed on the fracture surfaces of the prior powder particles, as can be seen in Fig. 3. Also, the bulk amorphous alloys show excellent corrosion resistance in both acid and seawater [60].

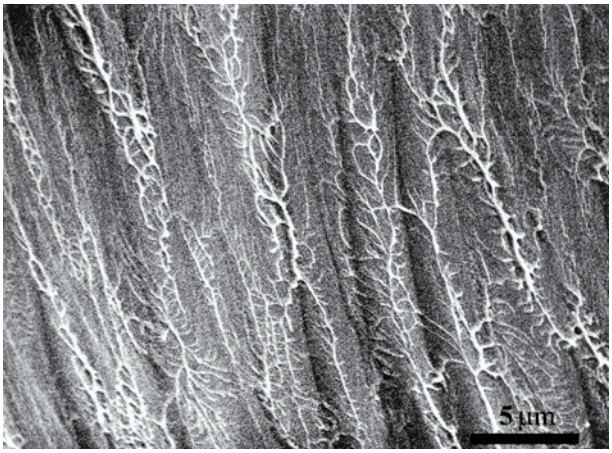

Fig. 3. Fracture surface of the $Ni_{59}Zr_{20}Ti_{16}Si_2Sn_3$. amorphous alloy fabricated by warm process.

Besides the MCAs mentioned above, ternary alloys such as Ni-Nb-(Sn [29], Ti [30], Ta [31]) have been reported to have a GFA high enough to form BMGs. These simple ternary alloys are more suitable for commercial use, and provide a good opportunity for the study of glass-forming mechanisms. In the case of Ni-Nb-Ta alloys, a fully amorphous rod with diameter of 2 mm is fabricated by injection casting $Ni_{60}Nb_{30}Ta_{10}$ alloy. The compressive failure strength of the $Ni_{60}Nb_{30}Ta_{10}$ BMG is 3346 MPa. As shown in Table 1, Ni-Nb-Ta MGs exhibit the highest level of glass transition and crystallization temperatures among the Ni-based BMGs reported to date. Since the melting range shifts to a higher temperature range with increasing Ta content, the improvement of GFA can be attributed to the significantly improved thermal stability of the amorphous phase against crystallization when a part of Nb is substituted with Ta.

5. Cu-BASED BMGS

Cu-Ti-Zr-Ni alloys have been reported to show a large SLR before crystallization and a high GFA [8]. BMG specimens with a thickness of 4 mm have been successfully produced by injection casting into a Cu mold. The CCR for amorphous formation is about 250 K/s for this alloy system. A small Si addition in Cu-Ti-Zr-Ni alloys even further stabilizes the super-cooled liquid against crystallization [61]. Further enhancement of GFA has been obtained by addition of Sn [62]. Fig. 4 shows a map of the phases for a bulk specimen as a function of rod diameter and alloy composition, determined by X-ray diffraction experiments; the symbols ○, ◑, and ● represent the amorphous phase, an amorphous and crystalline phase mixture, and crystalline phases, respectively. $Cu_{47}Ti_{33}Zr_{11}Ni_8Si_1$ has been reported to show a maximum diameter of 4 mm for amorphous formation. With increasing Sn content, the maximum diameter, increases up to 6 mm at x=2, followed by a decrease. The results clearly

Table 1. Glass transition and crystallization temperatures and critical diameter for bulk glass formation reported in Ni-Nb based amorphous alloys

Alloy system	T_g(K)	T_x(K)	Heating rate(K/s)	Critical diameter (mm)	References
$Ni_{65}Nb_5Cr_5Mo_5P_{14}B_6$	703	753	0.67	1	[4]
$Ni_{60}Nb_{20}Ti_{15}Zr_5$	841	898	0.67	2	[86]
$Ni_{60}Nb_{20}Ti_{12.5}Hf_{7.5}$	848	908	0.67	1.5	[87]
$Ni_{53}Nb_{20}Ti_{10}Zr_8Co_6Cu_3$	846	897	0.67	3	[88]
$Ni_{59.35}Nb_{34.45}Sn_{6.2}$	882	930	0.33	3	[27]
$Ni_{60}Nb_{36}Sn_3B_1$	882	940	0.33	3	[27]
$Ni_{60}Nb_{25}Ti_{15}$	857	904	0.67	1.5	[28]
$Ni_{60}Nb_{30}Ta_{10}$	934	961	0.67	2	[29]
$Ni_{60}Nb_{20}Ta_{20}$	*	994	0.67	-	[29]

*Cannot be measured due to the temperature limit in the DSC equipment

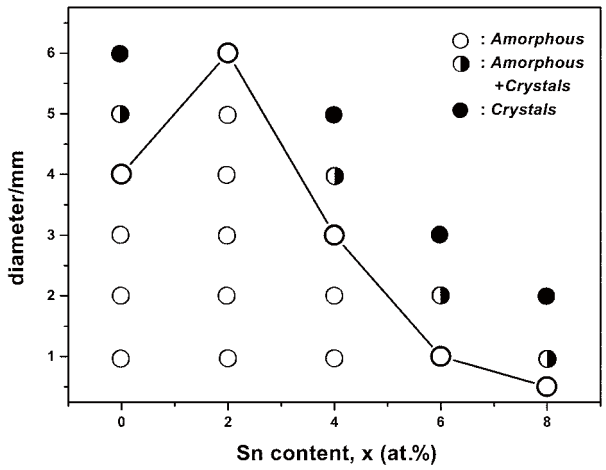

Fig. 4. Phase map describing the structure of bulk specimen with Sn content x in $Cu_{47}Ti_{33}Zr_{11}Ni_{8-x}Sn_xSi_1$ (x=0, 2, 4, 6, 8) alloys: ○, amorphous phase; ◑, amorphous and crystalline phase mixture; ●, crystalline phase.

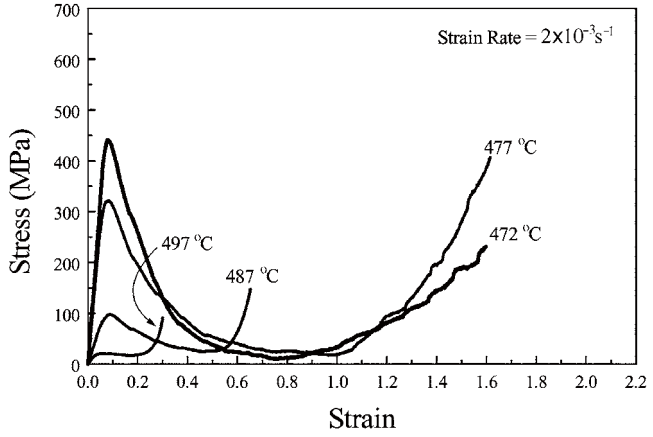

Fig. 5. Stress vs. stain curves obtained at several different temperatures between 447~497 ºC at a strain rate of $2\times10^{-3}s^{-1}$ for the $Cu_{47}Ti_{33}Zr_{11}Ni_6Sn_2Si_1$ glassy sheet.

show that the glass formation can be improved by partial substitution of Ni by Sn. The measured maximum diameter of the amorphous rod is in good correlation with the reduced glass transition temperature ($T_{rg}=T_g/T_l$, T_g: glass-transition temp., T_l: liquidus melting temp.) rather than SLR ΔT_x ($\Delta T_x=T_x-T_g$, T_x: crystallization temp.), at least in this alloy system. Fig. 5 shows flow stress vs strain curves obtained at several different temperatures in the SLR [63]. With increasing test temperature, flow stress decreases, as anticipated. The flow stress reaches a peak just after yielding and then decreases significantly with increasing strain. After the flow stress reaches the minimum plateau level, it rises again before failure. Also it has been confirmed that deformation in the supercooled liquid state accelerates the crystallization kinetics.

Partial substitution of Ni by In in $Cu_{47}Ti_{33}Zr_{11}Ni_8Si_1$ promotes the GFA [64]. $Cu_{47}Ti_{33}Zr_{11}Ni_6In_2Si_1$ BMG with a diameter of 6 mm can successfully be fabricated by a Cu-mold injection casting method. Partial substitution of Zr by Nb in $Cu_{47}Ti_{33}Zr_{11}Ni_8Si_1$ alloy improves the GFA and mechanical properties [65]. The $Cu_{47}Ti_{33}Zr_7Nb_4Ni_8Si_1$ alloy enables the fabrication of BMG with a diameter of 5 mm by the Cu-mold injection casting method. The compressive fracture strength (σ_f) and fracture elongation (ε_f) were 2.17 GPa and 6.05 %, respectively.

6. Ti-BASED BMGS

Large values of SLR ΔT_x (>50 K) have been reported in Ti-Cu-Ni-Sn amorphous alloys. Zhang *et. al.* reported a large value of ΔT_x (60 K) in the amorphous $Ti_{50}Cu_{25}Ni_{20}Sn_5$ alloy [66]. Kim et. al. further extended the SLR to a ΔT_x of 73 K for amorphous $Ti_{50}Cu_{32}Ni_{15}Sn_3$ alloy [9]. Further extension of GFA has been obtained by addition of Be [67]. Be can improve the GFA due to its small atomic size and the strong interaction between Ti and Be. A cast $Ti_{50}Cu_{32}Ni_{15}Sn_3$ cylinder with a diameter of 2 mm consists of an amorphous phase containing a small amount of crystalline phase. However, in the case of $Ti_{50}Cu_{25}Ni_{15}Sn_3Be_7$ and $Ti_{45}Cu_{25}Ni_{15}Sn_3Be_7Zr_5$ alloys, fully amorphous cylinder samples with diameters of 3 and 5 mm, respectively, have been successfully obtained. The improved GFA can be explained in terms of a decrease of the liquidus temperature and the tendency of the formation of short range order (SRO). The compressive fracture strength, Young's modulus, and total elongation are 2231 MPa, 53.1 GPa, and 4.2 %, respectively, for the $Ti_{50}Cu_{25}Ni_{15}Sn_3Be_7$ specimen, and 2328 MPa, 68.4 GPa, and 3.4 %, respectively, for the $Ti_{45}Cu_{25}Ni_{15}Sn_3Be_7Zr_5$ specimen. The fracture surface consists of a well-developed vein pattern.

The Ti-Zr-Be-Cu-Ni alloy system has been reported to form a fully amorphous phase or several phases, [i.e. β-Ti(Zr, Ni, Cu) phase or an icosahedral quasicrystalline phase embedded in the metallic glass matrix], depending on the alloys composition. Fig. 6 shows the composition range enabling formation of BMG (>1 mm and >6 mm dia.) by the Cu-mold injection casting method in the Ti-Zr-Be-Cu-Ni alloy system. For example, $Ti_{40}Zr_{29}Cu_8Ni_7Be_{16}$ BMG with a diameter up to 6 mm is fabricated by the Cu-mold injection casting method. In particular, $Ti_{40}Zr_{21}Cu_{10}Ni_9Be_{20}$ BMG enables the fabrication of BMG with a diameter of 10 mm by the Cu-mold injection casting method.

7. BMG MATRIX COMPOSITES

As noted earlier, one method to provide a global ductility to BMG is to produce a composite microstructure, consisting of crystalline and amorphous phase. The second crystalline phase distributed in the amorphous matrix may act as an initiation site of shear band, resulting in multiple shear band formation throughout the specimen and confinement of the

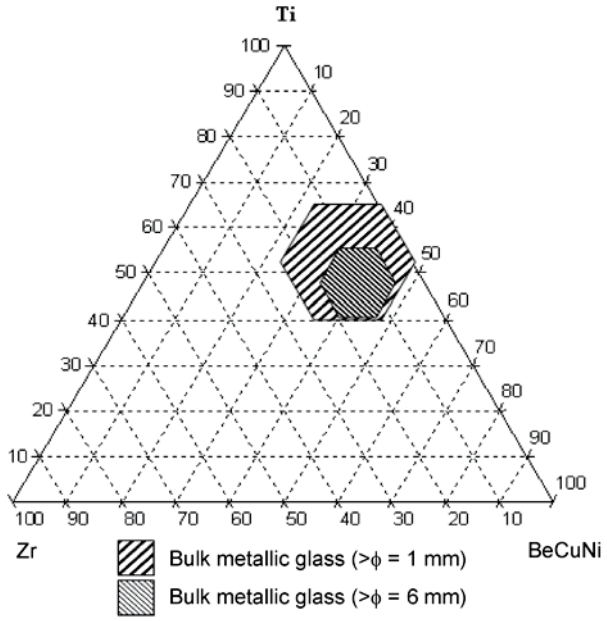

Fig. 6. Composition range enabling for the formation of BMG (>1 mm and >6 mm dia.) by Cu-mold injection casting method in Ti-Zr-Be-Cu-Ni alloy system.

propagation of the shear band [68-71]. One effective means to obtain a composite microstructure is to precipitate the nano-scale crystalline phase through a partial crystallization of the BMGs. Unfortunately, structural relaxation or precipitation of the crystalline phase from the amorphous matrix during annealing makes the specimen more brittle than the as-cast amorphous specimen.

Precipitation of a quasicrystalline phase from the amorphous matrix during annealing has been reported in many alloy systems such as Pd-U-Si [72,73], Al-based [74,75], Ti-based [76], and Zr-based [77,78] alloys. Formation of quasicrystalline phase in the BMG forming alloys has recently attracted significant interest, because strength and ductility of the BMG can be enhanced by precipitation of nano-scale quasicrystalline phase in the amorphous matrix. To date, improvement of the mechanical properties by precipitation of the quasicrystalline phase has been reported in Zr-based BMG forming alloy systems such as Zr-Al-Ni-Cu-Ag [79,80], Zr-Al-Ni-Cu-Pd [81], and Zr-Ti-Cu-Ni-Al [82]. Recently, it has been found that a stable icosahedral phase precipitates upon annealing of Ti-rich Ti-Zr-Be-Cu-Ni BMG [83]. Table 2 shows the effects of quasicrystalline phase precipitation upon annealing of the amorphous phase on the mechanical behavior of bulk glass forming Ti-Zr-Be-Cu-Ni alloy. The date clearly indicate that *in-situ* composites in which nano-sized quasicrystals are isolated and homogeneously distributed in an amorphous matrix exhibit simultaneous improvement in strength and ductility [84].

The simultaneous increase of the strength and global compressive strain by a partial crystallization of the amorphous phase indicates that the number of shear bands increased. The nano-sized quasicrystalline particles can act as either a nucleation site for the shear band formation or a barrier to the propagation of the shear bands, leading to an increase of yield strength and fracture strength. The nature of the interface is one of the factors in determining the mechanical properties of the composite alloys. A high interfacial strength between the crystalline phase and amorphous matrix can prevent shear band propagation effectively without crack initiation, and can act as a source for generating multiple shear bands. The Fourier filtered high resolution image showing the atomic structure of the interface between partially crystallized Ti-Zr-Be-Cu-Ni BMG (Fig. 7) clearly indicates a gradual structural change from a quasicrystal to amorphous structure at the interface. Due to the structural similarity between the quasicrystalline phase and amorphous phase, the interface energy between the quasicrystalline phase and

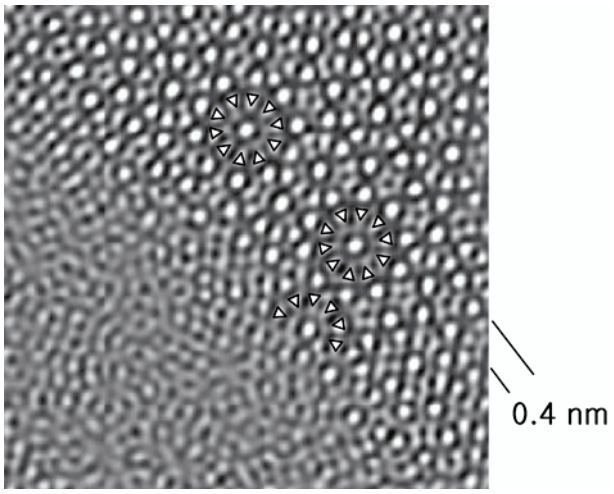

Fig. 7. High resolution TEM image of quasicrystal/amorphous interface in partially quasicrystallized $Ti_{40}Zr_{29}Cu_8Ni_{17}Be_{16}$ alloys.

Table 2. Mechanical properties of the as-cast amorphous and partially crystallized $Ti_{40}Zr_{29}Cu_8Ni_7Be_{16}$ alloy rods: Youngs modulus E, yield stress σ_y, ultimate compression stress σ_{max}, yield strain ε_y and fracture strain ε_f

Fraction of quasicrystal	E (Gpa)	σ_y (MPa)	σ_{max} (MPa)	ε_y (%)	ε_f (%)
0 %	96	1893	1921	2.0	5.1
7 %	106	2038	2084	1.9	6.2
21 %	101	1911	2005	1.9	3.4
35 %	131	1978	2026	1.5	1.7
70 %	139	1876	1876	1.4	1.4

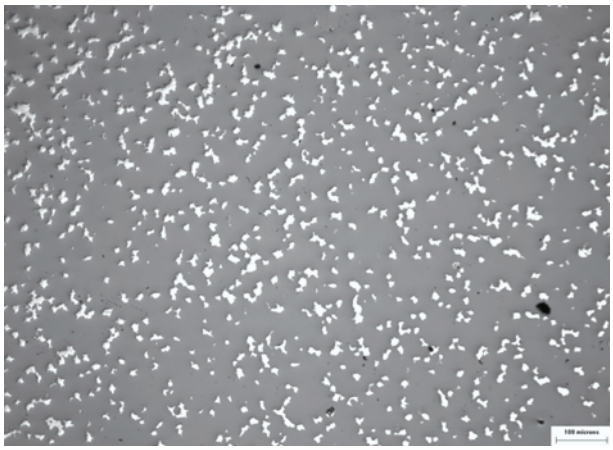

Fig. 8. Optical micrograph of the BMG composite containing 20 vol.% brass on the cross-section. The brass powders are well distributed in the metallic glass matrix.

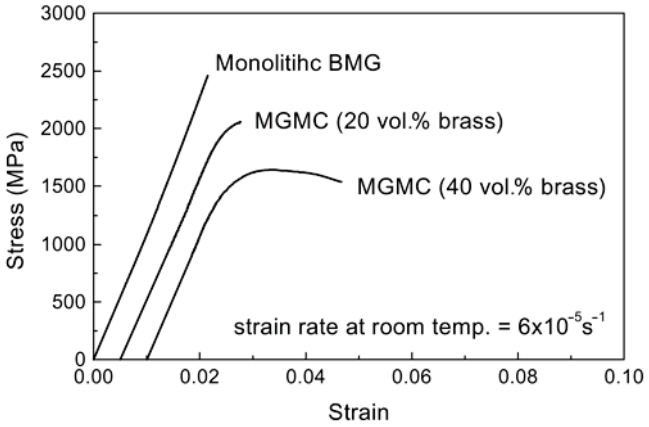

Fig. 9. Stress vs. strain curves of the monolithic sample and BMG composites containing 20 vol.% brass and 40 vol.% brass tested under uniaxial compressive condition at room temperature. The load is applied along the extrusion direction.

the amorphous phase is presumed to be lower than that between the crystalline phase and the amorphous phase, leading to a simultaneous increase of strength and ductility.

The ductility of the bulk amorphous alloys can be improved by incorporating a ductile phase in the amorphous matrix. Fig. 8 shows the microstructure of a ductile brass phase dispersed in a $Ni_{59}Zr_{20}Ti_{16}Si_2Sn_3$ amorphous matrix composite fabricated by the warm extrusion method [85]. Fig. 9 compares the stress vs. strain curves obtained from the ductile brass phase dispersed in BMG matrix composites, indicating that catastrophic failure can be avoided by introducing a ductile second phase in the metallic glass matrix. As shown in Fig. 10, many shear bands initiate from the elongated brass powders during compressive loading. There is a clear tendency that the shear bands do not pass through the neighboring brass powders but remain confined between them. Upon yielding of the BMG matrix composites, the soft brass phase deforms plastically first, and then load is transferred to the

Fig. 10. Optical images taken from the outer surface of the failed BMG composite containing 40 vol.% brass; many shear bands are initiated from the interface between brass-fibers and the matrix, but they do not propagate through the neighboring brass-fibers.

surrounding glass matrix, causing initiation of shear bands at several places along the brass-fiber/matrix interface. The initiated shear bands propagate but interact with neighboring brass powders. The propagation of single shear bands is found to be restricted to the volume between the brass powders and further propagation through the brass powder is prevented. This behavior is quite similar to that of finely dispersed *in-situ* ductile phase reinforced bulk metallic glass composites. However, the size and spacing between the powders is much larger in such a microstructure system. Due to the initiation and confinement of shear bands, the BMG matrix composites do not fail catastrophically by a single shear band propagating through the whole sample in a monolithic sample. Instead, plasticity is distributed more homogeneously in the form of shear band patterns, which results in higher strains to failure.

6. SUMMARY

Significant progress has been made in enhancing the glass forming ability of Ca-, Mg-, Ni-, Cu-, and Ti-based alloys. Further increase in the achievable dimensions is possible through warm processing of the amorphous alloy powders in the wide super-cooled liquid region. Improvement of ductility by the successful synthesis of *in-situ* and *ex-situ* BMG matrix composites suggests that high strength and corrosion resistant bulk amorphous materials can be utilized in the near future.

ACKNOWLEDGMENTS

This research was supported by the Creative Research Initiatives project of the Korean Ministry of Science and Technology.

REFERENCES

1. W. Klement, R. H. Willens, and P. Duwez, *Nature* **187**, 869 (1960).
2. A. Inoue, *Acta mater*. **48**, 279 (2000).
3. A. Inoue and T. Zhang, *Mater. Trans.* **37**, 185 (1996).
4. X. Wang, I. Yoshii, A. Inoue, Y. H. Kim, and I. B. Kim, *Mater. Trans.* **40**, 1130 (1999).
5. A. Inoue, N. Nishiyama, and T. Matsuda, *Mater.Trans.* **37**, 181 (1996).
6. H. K. Lim, S. Yi, W. T. Kim, D. H. Kim, S. H. Kim, and N. J. Kim, *Scripta mater*. **44**, 1635 (2001).
7. Y. C. Jung and K. Nakai, *Met. Mater. -Int.* **9**, 337 (2003).
8. X. H. Lin and W. L. Johnson, *J. Appl. Phys*. **78**, 6514 (1995).
9. Y. C. Kim, S. Yi, W. T. Kim, and D. H. Kim, *Materials Science Forum* **360-362**, 67 (2001).
10. E. S. Park and D. H. Kim, *J. Mater. Res.* **19**, 685 (2004).
11. H. G. Kang, E. S. Park, W. T. Kim, D. H. Kim, and H. K. Cho, *Mater.Trans.* **41**, 846 (2000).
12. G. He, J. Eckert, and W. LÖser, *Acta mater*. **51**, 1630 (2003).
13. G. He, J. Eckert, W. Löser, and L. Schultz, *Nature Mater*. **2** , 33 (2003).
14. H. Choi-Yim, R. Busch, U. Köster, and W. L. Johnson, *Acta mater*. **47**, 2455 (1999).
15. C. P. Kim, R. Bush, A. Masuhr, H. Choi-Yim, and W. L. Johnson, *Appl. Phys. Lett*. **79**, 1456 (2001).
16. C. Fan, R. T. Ott, and T. C. Hufnagel, *Appl. Phys. Lett*. **81**, 1020 (2002).
17. G. He, W. Löser, and J. Eckert, *Scripta mater*. **48**, 1531 (2003).
18. C. C. Hays, C. P. Kim, and W. L. Johnson, *Phys. Rev. Lett*. **84**, 2901 (2000).
19. F. Szuecs, C. P. Kim, and W. L. Johnson, *Acta mater*. **49**, 1507 (2001).
20. J. K. Lee, S. H. Kim, W. T. Kim, and D. H. Kim, *Met. Mater. -Int.* **7**, 187 (2001).
21. G. He, W. LÖser, J. Eckert, and L. Schultz, *J. Mater. Res*. **17**, 3015 (2002).
22. Y. Kawamura, H. Kato, A. Inoue, and T. Masumoto, *Int. J. Powder Met*. **30**, 50 (1997).
23. T. Zhang and A. Inoue, *Mater. Trans.* **40**, 301 (1999).
24. S. Yi, T. G. Park, and D. H. Kim, *J. Mater. Res*. **15**, 2429 (2000).
25. D. J. Sordelet, E. Rozhkova, P. Huang, P. B. Wheelock, M. F. Besser, M. J. Kramer, M. Calvo-Dahlborg and U. Dalhborg, *J. Mater. Res*. **17**, 186 (2002).
26. M. H. Lee, D. H. Bae, W. T. Kim, D. H. Kim, and D. J. Sordelet, *J. Non-Cryst. Solids* **315**, 89 (2003).
27. A. Inoue, W. Zhang, T. Zhang, K. Kurosaka, *Acta mater*. **49**, 2645 (2001).
28. A. Inoue and W. Zhang, *Mater. Trans*. **43**, 2921 (2002).
29. H. Choi-Yim, D. H. Xu, and W. L. Johnson, *Appl. Phys. Lett*. **82**, 1030 (2003).
30. W. Zhang, A. Inoue, *Mater. Trans*. **43**, 2342 (2002).
31. M. H. Lee, D. H. Bae, W. T. Kim, and D. H. Kim, *Mater. Trans*. **44**, 2084 (2003).
32. A. Inoue, T. Nakamura, N. Nishiyama, and T. Masumoto, *Mater. Trans*. **33**, 937 (1992).
33. H. Men and D. H. Kim, *J. of Mater. Res*. **18**, 1502 (2003).
34. K. Amiya and A. Inoue, *Mater. Trans.* **43**, 81 (2002).
35. K. Amiya and A. Inoue, *Mater. Trans*. **43**, 2578 (2002).
36. J.-H. Kim, J. S. Park, E. S. Park, W. T. Kim, and D. H. Kim, *Mat. Mater. -Int.* in press.
37. P. Villars, A. Prince, and H. Okamoto, *Handbook of Ternary Alloy Phase Diagrams* **6** (eds., Thaddeus B. Massalski), p. 7522, ASM, Materials Park, OH (1995).
38. A. Inoue, T. Negishi, H. M. Kimura, T. Zhang, and R. Yavari, *Mater. Trans.* **39**, 318 (1998).
39. E. S. Park, W. T. Kim, and D. H. Kim, *J. Non-Cryst. Solids* submitted.
40. S. G. Kim, A. Inoue, and T. Masumoto, *Mater. Trans*. **31**, 929 (1990).
41. A. Inoue, A. Kato, T. Zhang, S. G. Kim, and T. Masumoto, *Mater. Trans*. **32**, 609 (1991).
42. A. Inoue, T. Nakamura, N. Nishiyama, and T. Masumoto, *Mater. Trans*. **33**, 937 (1992).
43. E. S. Park, H. G. Kang, W. T. Kim and D. H. Kim, *J. Non-Cryst. Solids* **279**, 154 (2001).
44. K. Amiya and A. Inoue, *Mater. Trans*. **41**, 1460 (2000).
45. K. Amiya and A. Inoue, *Mater. Trans*. **42**, 543 (2001).
46. H. Men, Z. Q. Hu, and J. Xu, *Scripta. mater*. **46**, 699 (2002).
47. F. E. Luborsky, *Amorphous Metallic Glass*, p.4, Butterworths, London, UK (1983).
48. R. P. Messmer, *Phys. Rev. B* **23**, 1616 (1981).
49. J. L. Walter, *Mater. Sci. Engi*. **39**, 95 (1979).
50. I. Vincze, D. S. Boudreaux, and M. Tegze, *Phys. Rev. B* **19**, 4896 (1979).
51. I. Vincze, F. Van der Woude, T. Kemeny, and A.S. Schaafsma, *J. Magnetism magn. Mater.* **15-18**, 1336 (1980).
52. D. V. Louzguine and A. Inoue, *J. Mater. Res.* **17**, 2112 (2002).
53. H. Men, W. T. Kim, and D. H. Kim, *Mater. Trans*. **44**, 2141 (2003).
54. E. S. Park, W. T. Kim, and D. H. Kim, *Mater. Trans*. **45**, 2474 (2004).
55. T. G. Park, S. Yi, and D. H. Kim, *Scripta mater.* **43**, 109 (2000).
56. W. B. Kim, B. J. Ye, and S. Yi, *Met. Mater. -Int.* **10**, 1 (2004).
57. A. Inoue, *Acta mater*. **48**, 279 (2000).
58. J. K. Lee, D. H. Bea, S. Yi, W. T. Kim, and D. H. Kim, *J. Non-Crst. Solids* **333**, 212 (2004).
59. J. Y. Lee, D. H. Bae, J. K. Lee, and D. H. Kim, *J. Mater. Res*. **19**, 2221 (2004).
60. S. J. Pang, T. Zhang, K. Asami, and A. Inoue, *Acta mater*. **50**, 489 (2002).
61. H. Choi-Yim, R. Bush, and W. L. Johnson, *J. Appl. Phys*. **83**, 7993 (1998).
62. E. S. Park, H. K. Lim, W. T. Kim, and D. H. Kim, *J. Non-Cryst. Solids* **298**, 15 (2002).

63. D. H. Bae, H. K. Lim, S. H. Kim, D. H. Kim, and W. T. Kim, *Acta mater*. **50**, 1749 (2002).
64. E. S. Park, W. T. Kim, and D. H. Kim, *Mater. Trans*. **45**, 2693 (2004).
65. E. S. Park, D. H. Kim, T. Ohkubo, and K. Hono, *J. Non-Cryst. Solids*, Submitted.
66. T. Zhang and A.Inoue, *Mater. Trans.* **39**, 1001 (1998).
67. Y. C. Kim, W. T. Kim, and D. H. Kim, *Mater. Tran*. **43**, 1243 (2002).
68. J. Eckert, A. Reger-Leonhard, B. Weiß, and M. Heilmaier, *Mater. Sci. Eng*. *A* **301**, 1 (2001).
69. A. Inoue, T. Zhang, M. W. Chen, and T. Sakurai, *J. Mater. Res*. **15**, 2195 (2000).
70. R. D. Conner, R. B. Dandliker, and W. L. Johnson, *Acta mater*. **46**, 6189 (1998).
71. H. Choi-Yim and W. L. Johnson, *Appl. Phys. Lett*. **71**, 3808 (1997).
72. S. J. Poon, A. J. Drehman, and K. R. Lawless, *Phys. Rev. Lett*. **55**, 2324 (1985).
73. Y. Chen, S. J. Poon, and G. J. Shiflet, *Phys. Rev. B* **34**, 3516 (1986).
74. A. P. Tsai, A. Inoue, Y. Bizen, and T. Masumoto, *Acta metall*. **37**, 1443 (1989).
75. J. C. Holzer and K. F. Kelton, *Acta metall*. **39**, 1833 (1991).
76. V. V. Molokanov and V. N. Chebotnikov, *J. Non-Cryst. Solids* **117/118**, 789 (1990).
77. U. Köster, J. Meinhardt, S. Roos, and H. Liebertz, *Appl. Phys. Lett*. **69**, 179 (1996).
78. J. K. Lee, G. Choi, W. T. Kim, and D. H. Kim, *Appl. Phys. Lett*. **77**, 978 (2000).
79. A. Inoue, T. Zhang, J. Saida, and M. Matsushita, *Mater. Trans.* **41**, 1511 (2000).
80. T. K. Han, S. J. Kim, Y. S. Yang, A. Inoue, Y. H. Kim, and I. B. Kim, *Met. Mater. -Int.* **7**, 91 (2001).
81. A. Inoue, C. Fan, J. Saida, and T. Zhang, *Sci. Tech. Advanced Materials* **1**, 73 (2000).
82. L. Q. Xing, J. Eckert, and L. Schultz, *NanoStructured materials*, **12**, 503 (1999).
83. Y. C. Kim, J. M. Park, J. K. Lee, W. T. Kim, and D. H. Kim, *Mater. Trans*. **44**, 1978 (2003).
84. Y. C. Kim, J. H. Na, J. M. Park, D. H. Kim, and W. T. Kim, *Appl. Phys. Lett*. **83**, 3093 (2003).
85. D. H. Bae, M. H. Lee, D. H. Kim, and D. J. Sordelet, *Appl. Phys. Lett*., **83**, 2312 (2003).
86. A. Inoue, W. Zhang, and T. Zhang, *Mater. Trans.* **43**, 1952 (2002).
87. W. Zhang and A. Inoue, *Scripta mater.* **48**, 641 (2003).
88. T. Zhang and A. Inoue, *Mater. Trans.* **43**, 708 (2002).